DOI: 10.13009/EUCASS2017-495

Duplication of reacting boundary layer between hypersonic flight and Plasmatron facility

Jean-Etienne Durand, Alan Viladegut, Fabio Pinna and Olivier Chazot
von Kármán Intitute for Fluid Dynamics,
Chaussée de Waterloo, 72 B-1640 Rhode-St-Genèse Belgium
jean-etienne.durand@onera.fr*
alan.viladegut@vki.ac.be

Abstract

In re-entry, spacecrafts require a Thermal Protection System (TPS) to withstand severe heat flux conditions on the surface. The most critical thermal load is located at the stagnation point, becoming the TPS design reference. Nevertheless, the design can be improved at off-stagnation through a new extrapolation methodology that duplicates in high enthalpy facilities the reacting boundary layer found in flight. The present work assesses the effects of the vehicle's body curvature on the heat flux by reproducing locally the reacting boundary layer of the Intermediate eXperimental Vehicle (IXV) at a specific point of an equivalent flat plate. The methodology application on the flat plate model available at VKI is also investigated.

1. Introduction

Thermal Protection Systems (TPS) are critical to protect the spacecraft from the extreme conditions encountered during atmospheric re-entry. TPS materials are characterized on ground under flow conditions closely related to the flight. However, not all the phenomena appearing in hypersonic regimes can be fully reproduced with one single ground facility.[1] The way to overcome such issue is the partial simulation method, in which only some relevant characteristics of the flight environment are reproduced in dedicated facilities on ground, depending on the specific phenomenon taken into consideration.

Many TPS designs are based on a prediction of the stagnation point heat flux because it is considered as the most critical point over the vehicle. In harmony with industry requirements, Kolesnikov[2] proposed a flight-to-ground extrapolation methodology for high enthalpy facilities known as the Local Heat Transfer Simulation (LHTS), which applies to stagnant flows and is able to provide the same thermo-chemical boundary layer on both the flying body and its equivalent model on ground. However, farther downstream of the stagnation point, the TPS does not face such extreme thermal conditions and the aerospace industry could also benefit from a more optimized TPS design that allows either increasing the payload or reducing the cost of the mission. Following this idea, Barbante[3] extended the extrapolation methodology to a more general off-stagnation point configuration. He derived the boundary layer equations for shear flow and proposed the boundary layer reproduction across simple geometries such as spheres or flat plates. Then, Viladegut et al.[4] provided its validation over a flat plate model using the Plasmatron facility in the von Karman Institute for Fluid Dynamics (VKI).

The present work aims at applying the extrapolation method to a more generic flying body configuration such as the Intermediate eXperimental Vehicle (IXV). The paper attempts to establish a similitude strategy for the non-equilibrium boundary layer between IXV's windward side and a flat plate model that can be installed in a plasma wind tunnel. The activity will enhance the VKI capabilities to experimentally validate aerothermodynamic models in the VKI-Plasmatron facility using flight data from the IXV re-entry mission.

The off-stagnation point extrapolation methodology considers two geometric effects for heat flux duplication: the curvature and the size of the re-entry body. These effects will be treated hereafter independently, and the extrapolation will be applied in two steps. The former extrapolates the boundary layer profile at a specific location on the IXV's

*Currently PhD candidate at ONERA, J.E. Durand did the research master of the von Kármán Institute for fluid dynamics (2015-2016).

DOI: 10.13009/EUCASS2017-495

windward side to an equivalent flat plate, while the latter scales down the flow around the equivalent flat plate into another flat plate that fits the plasma wind tunnel model requirements.

2. Bondary layer considerations at off-stagnation point

The LHTS is a heat flux duplication methodology based on the stagnation point heat flux equations proposed by Fay and Riddell[5] and Goulard[6] in the late 50's. The LHTS concept states that, by preserving the parameters appearing in the heat flux equations between flight and ground configurations, the boundary layer profile can be reproduced at stagnation point. Barbante[3] extended this approach for boundary layers at off-stagnation point by deriving the equations using the Lees-Dorodnitsyn coordinate transformation:

$$\xi = \int_0^s \rho_\delta \mu_\delta u_\delta r^{2\epsilon} dx \quad \text{and} \quad \eta = \frac{u_\delta r^\epsilon}{\sqrt{2\xi}} \int_0^y \rho dy \tag{1}$$

Where ϵ=0 applies to two-dimensional flow and ϵ=1 to axisymmetric flow. Assuming local self-similarity by neglecting the derivatives with respect to ξ from the derivatives with respect to η, the heat flux transferred to the wall can be expressed by:

$$q_w = 0,332 \frac{\rho_\delta \mu_\delta u_\delta r^\epsilon}{Pr^{2/3}\sqrt{\xi}} \left(h_{t,\delta} - h_{t,w}\right) \left(1 + \frac{u_\delta^2 (Pr-1)}{4\left(h_{t,\delta} - h_{t,w}\right) Pr^{1/4}} + \frac{Le-1}{Le^{1/3}} \left[1 + 0,47 \left(\frac{Pr}{Le}\right)^{\frac{1}{3}} \frac{1}{Da_w}\right]^{-1} \frac{\left[c_{A,\delta} + Da_g G_\delta\right] \Delta h_A}{h_{t,\delta} - h_{t,w}}\right) \tag{2}$$

where $\rho_\delta, \mu_\delta, u_\delta, h_{t,\delta}, G_\delta, h_{t,w}$ are the density, the dynamic viscosity, the velocity, the total enthalpy and the chemical reaction rates, respectively. Note that subscripts δ and w refer to the flow property at the boundary layer outer edge and at the wall of the body. Da_g and Da_w are the gas phase and the heterogeneous Damköhler numbers, respectively. Le and Pr are the Lewis and the Prandtl numbers. The last parameter is the flight condition factor f_c, a mathematical parameter strongly related to the lagrangian time of the flow (Barbante[3] & Chazot et al.[7]), defined as:

$$f_c = \frac{u_\delta r^\epsilon}{\sqrt{\xi}} \tag{3}$$

The flight condition factor f_c is a parameter which, consistently with the parabolic nature of the boundary layer equations, contains the flow history from the stagnation point to a specific wall-coordinate s on the body through its dependence with ξ. In consequence, f_c is strongly related to the boundary layer thickness δ and the typical boundary layer flow-time τ_f conditioning the gas-phase Damköhler number:

$$\delta = \frac{\sqrt{2}}{\rho_\delta f_c} \quad \text{and} \quad \tau_f = \frac{2Pr}{Le \rho_\delta u_\delta f_c^2} \tag{4}$$

Following the LHTS concept, if all the parameters appearing in eq. (2) are reproduced in flight and ground configurations, the same heat flux must be obtained in both cases. However, respecting the same outer edge velocity from the flight requires a model on ground with similar dimensions to those of the flying body. Considering the flat plate as the model on ground, the flight condition factor can be derived as $f_c \propto \sqrt{u_\delta / x}$. Thus, the duplication requirements of u_δ and f_c lead to the conclusion that the perfect boundary layer duplication can only be achieved if the flight velocity and size conditions from the flight are obtained in the laboratory. Nevertheless, a partial similitude is possible by relaxing the condition on velocity. Chazot et al.[7] stated that, considering the characteristics of the boundary layer along a re-entry vehicle, like for the IXV, with high angle of attack, the Mach number at the boundary layer edge does not go beyond 2, corresponding to low Eckert number regimes (eq. (5)):

$$Ec = \frac{u_\delta^2}{h_\delta} << 1 \tag{5}$$

Thus, under the hypothesis of low Ec numbers, the heat flux is dominated by thermochemical phenomena, and the velocity and total enthalpy reproduction on ground can be ignored, and the static enthalpy becomes the relevant parameter to consider. Hence, the reduction of both the flat plate length and the ground testing velocity is possible while f_c values remains the same. As the lagrangian time of the flow is thereby conserved and the chemistry time does not change, the Damköhler numbers are also duplicated. Barbante[3] observed that the maximum heat flux difference for the non-catalytic case is about 21% and for the fully catalytic case 19%, ranging from M_δ=0.1 to 2. Such discrepancies are due to viscous dissipation, which increases with the Mach number, inside the boundary layer. Despite those differences, the structure of the boundary layer was shown similar for all Mach number.

DOI: 10.13009/EUCASS2017-495

3. Heat flux extrapolation issues for complex configurations

A preliminar heat flux duplication strategy, between a complex configuration such as the IXV windward side and a flat plate, has been investigated at the VKI by Ledard.[8] The duplication was done by finding the location on the flat plate where the heat flux was the same as in the IXV. However, even though the heat flux could indeed be duplicated, thermochemical phenomena between the IXV and the flat plate significantly differed, as the methodology did not take into account the physical parameters appearing in the reacting boundary layer analysis proposed by Barbante.[3] To improve the TPS design and to validate aerothermodynamic models in plasma facilities, the full set of thermochemical phenomena should be duplicated rigorously between flight and ground. Therefore, a more elaborate duplication methodology is required for future ground testing at off-stagnation point.

The boundary layer duplication between hypersonic flight and ground testing is implicitly affected by two geometrical effects, as seen in figure 1:

- The curvature effect, which is manifested by the variation of pressure and could alter the boundary layer duplication results.
- The size effect, which was already studied for flat plates under the off-stagnation methodology proposed by Barbante.[3]

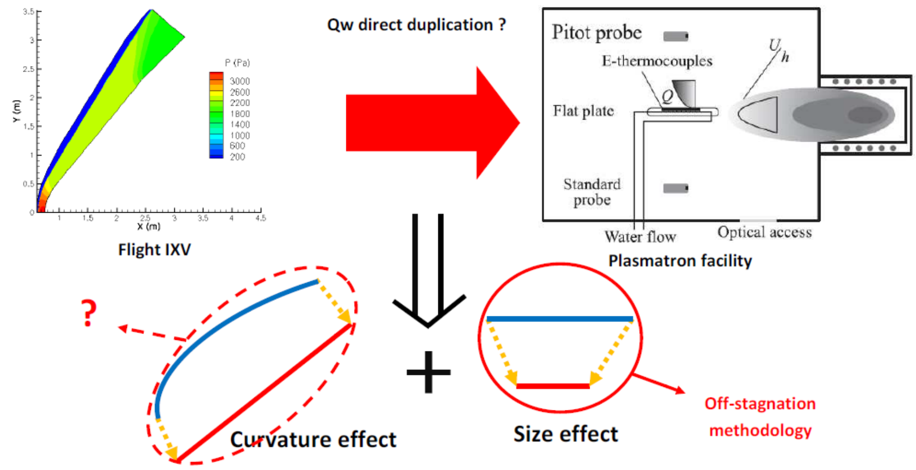

Figure 1: Geometrical effects over the heat flux duplication from hypersonic flight to Plasmatron facility.

Both geometrical effects must be studied separately for hypersonic boundary layer duplication in the Plasmatron facility. A methodology is proposed here and applied under chosen IXV flight conditions in two extrapolation steps, as seen in figure 2. The first one considers the curvature effects and duplicates locally the boundary layer found on the IXV at the end of an equivalent flat plate. Then, a second extrapolation procedure scales down the equivalent flat plate into a flat plate model that fits with Plasmatron testing constraints.

4. Application of the off-stagnation point extrapolation methodology

The first step considers the extrapolation of the reacting boundary layer from an IXV flight condition to an equivalent flat plate for assessing the curvature effects of the body shape. The second step carries out the off-stagnation methodology detailed in previous studies which reduces the size of the flat plate to fit with Plasmatron testing conditions.

4.1 First step: Curvature effects

The data extrapolation is realized in three sub-steps (figure 3). The data is first extracted at the outer-edge of the thermal boundary layer for a given point on the body surface and are used to specify the boundary conditions for the CFD simulations of the equivalent flat plate configuration. Then, the results are compared.

DOI: 10.13009/EUCASS2017-495

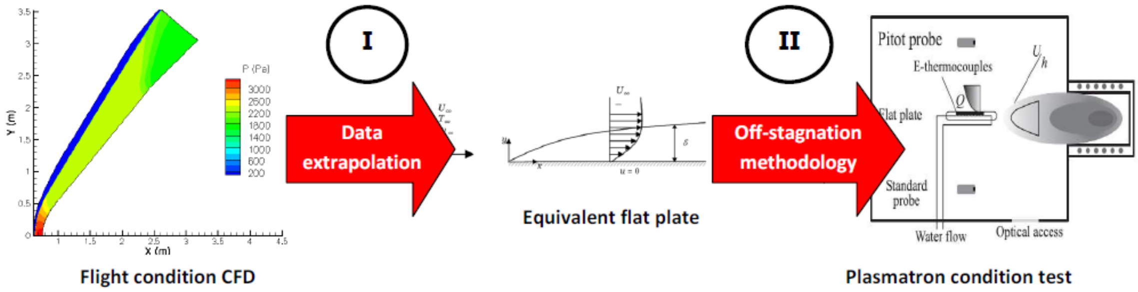

Figure 2: Methodology of the heat flux duplication from a re-entry vehicle windward side into the Plasmatron facility.

- **Extraction of extrapolation parameters**. Based on a numerical simulation of the IXV's windward side, for a given point at the surface of the body, the velocity, the temperature, the pressure and the chemical composition are extracted at the outer edge of the thermal boundary layer, which is defined by 99% of the difference of total enthalpy from the wall, following:

$$0.99 = \frac{H_t(s, \delta(s)) - H_{t,w}(s)}{H_{t,\infty}(s) - H_{t,w}(s)} \tag{6}$$

- **Design and CFD of an equivalent flat plate**. Ideally, on the flat plate configuration, the flow has the velocity, the pressure, and the temperature uniform and constant along the outer edge of the boundary layer. Based on this assumption, the inlet conditions for flat plate simulations are the same as those parameters extracted at the outer edge of the boundary layer on IXV.

  The point over an equivalent flat plate s_{eq}, at which the boundary layer profile is locally reproduced, is determined by reproducing the Lees-Dorodnitsyn coordinate abscissa for duplicating the flight factor, as the outer-edge velocity is reproduced. The integration of that coordinate must start from the stagnation point of the flat plate. In fact, as the boundary layer thickness must be finite, the velocity at $\xi = 0$ must be equal to zero (eq. (7)). Only at the stagnation point region, this condition is available.

$$u_\delta(\xi) \propto \frac{\delta\sqrt{2\xi}}{\int_0^1 \rho(\eta)\, d\eta} \quad \to \; 0 \quad \text{when} \quad \xi \to 0 \tag{7}$$

- **Comparison between flat plates and IXV computation results**. To assess the accuracy and the efficiency of the extrapolation methodology, the flight and the flat plate variables are compared using:

$$\frac{\Delta\phi}{\phi} = 100 \times \frac{(\phi_{IXV} - \phi_{fp})}{\phi_{IXV}} \tag{8}$$

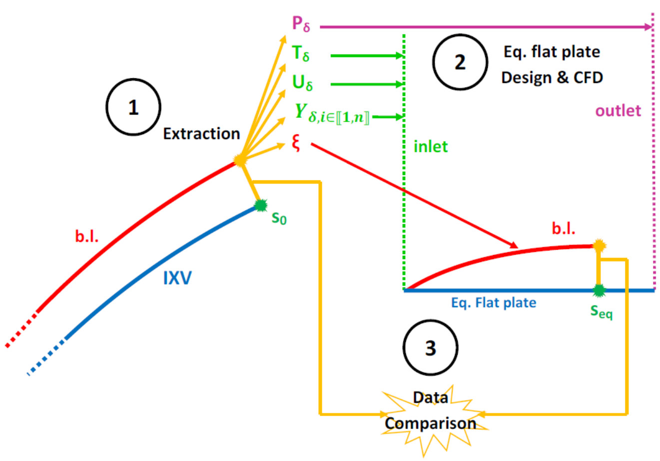

Figure 3: Data extrapolation process

DOI: 10.13009/EUCASS2017-495

After the first extrapolation step, the obtained results allow assessing the effects of curvature.

4.2 Second step: Scaling over a flat plate model

The equivalent flat plate is reduced to fit with the Plasmatron facility dimension by using the off-stagnation methodology between two plates, as proposed by Barbante.[3] The heat flux is compared with that obtained from the IXV simulation to obtain a global efficiency of the heat flux duplication of the full methodology.

4.3 Reference IXV re-entry simulation

The feasibility of the methodology is shown by taking as example the windward side of IXV. The full scale IXV vehicle is 5 m long, 1.5 m high and 2.2 m wide. The flight conditions are the same as those used by Ledard[8] and provided in table 1. The body is assumed to be in Earth atmospheric re-entry at an altitude of 60 km.

Table 1: IXV atmospheric re-entry case.

	P_∞ (Pa)	T_∞ (K)	$U_\infty\left(m.s^{-1}\right)$	Y_N	Y_O	Y_{O_2}	Y_{NO}	Y_{N_2}
IXV case at M = 20	6.13	222.44	5980.11	0	0	0.23	0	0.77

A 2D-symmetry along the stagnation line is applied to the 2D IXV geometry. The surface is low catalytic ($\gamma = 0.00694$) and the radiative equilibrium is assumed with an emissivity of 0.8. The 2D case is considered here as a first attempt to assess the methodology, but using 2D-axisymmetric and 3D simulations will be also of interest in the near future.

5. CFD simulation of the flow

The steady state computation of the hypersonic flow over the IXV windward side is made with the CFD++ solver from Metacomp Technologies with a 2D structured mesh (figure 4). The considered gas is ideal, with 5 different species (N, O, O_2, NO and N_2), and plugged into Park's chemical model.[9] Ionization phenomenon is not taken into account. The flow is assumed compressible and laminar. No turbulence model is introduced because Reynolds number is low enough in such conditions. As the pressure is low (<3400 Pa) and the temperature is below 6000 K, the shock layer can be considered optically thin. Hence, the radiation contribution to the heat flux is neglected.

For the geometry of the flat plate, it must take into account strong subsonic compressible effects. A thin flat plate, with a radius of 1 mm, enables the compression and the expansion regions to be confined close to the stagnation point, leaving the remaining part of the flat plate free of any pressure gradient. The entire length of the flat plate is equal to 2 meters. At the inlet, only temperature, velocity and mass fraction of species are imposed equal to the ones extracted from IXV simulations, as defined in the previous section. Similarly, static pressure is prescribed at the outlet. The same symmetry and wall conditions are chosen between the equivalent flat plate and IXV. Furthermore, the flow model, the reactions, assumptions about the gas, catalycity and the emissivity values are the same in the flat plate and the IXV simulations.

6. Numerical results

The comparison of numerical results from the IXV and flat plates computations assesses the curvature effect over the flight-to-ground extrapolation. Five points on the wall, whose coordinate starts from the stagnation point of the IXV, are chosen: case 1 (s = 20 cm), case 2 (s = 40 cm), case 3 (s = 60 cm), case 4 (s = 80 cm) and case 5 (s = 1 m). The studied zone contains, on the other hand, a strong variation of pressure because of the curvature and the proximity of the shock. Cases 1 and 2 are located in the region where the pressure gradient is strong. For the three other cases (3, 4 and 5), little variation of pressure is observed (figure 5). All cases are in subsonic regime (Mach number, table 2).

DOI: 10.13009/EUCASS2017-495

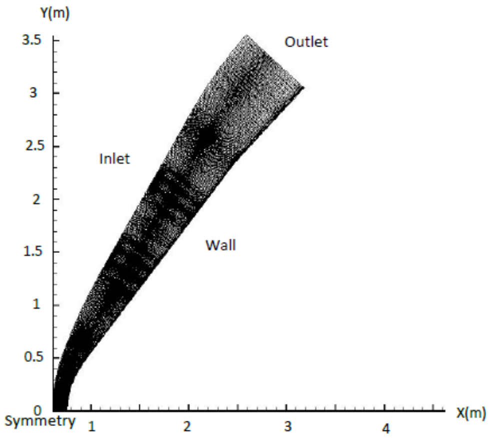

Figure 4: 2D mesh of the IXV windward.

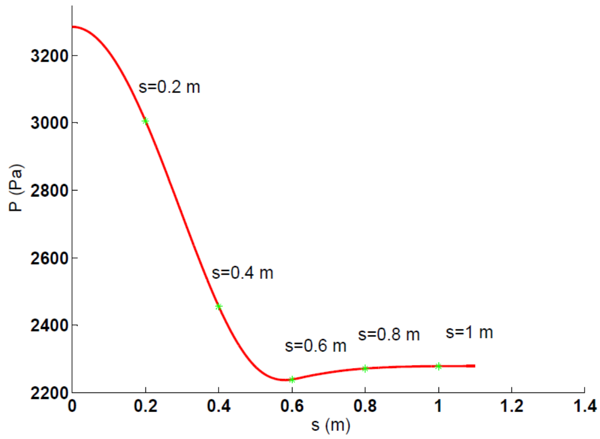

Figure 5: Pressure evolution along the outer-edge.

6.1 Curvature effects: results and discussion

For each case, pressure, temperature, velocity and species mass fractions at the outer edge of the IXV's boundary layer are provided in table 2. Their respective heat flux and the Lees-Dorodnitsyn abscissa are also given.

Table 2: Sample point cases on the IXV windward surface

Case	1	2	3	4	5
M_δ	0.37	0.68	0.79	0.78	0.79
P_δ (Pa)	3005	2456	2239	2271	2278
T_δ (K)	5608	5366	5279	5335	5362
U_δ $(m.s^{-1})$	659	1181	1362	1361	1377
$Y_{N,\delta}$	0.201	0.197	0.194	0.192	0.190
$Y_{O,\delta}$	0.228	0.229	0.229	0.229	0.229
$Y_{O_2,\delta}$	4.6×10^{-5}	3.2×10^{-5}	2.8×10^{-5}	3.2×10^{-5}	3.4×10^{-5}
$Y_{NO,\delta}$	0.003	0.003	0.002	0.003	0.003
$Y_{N_2,\delta}$	0.567	0.572	0.575	0.577	0.579
ξ $(kg^2.m^{-2}.s^{-2})$	9.8×10^{-6}	3.4×10^{-5}	6.3×10^{-5}	9.3×10^{-5}	1.2×10^{-4}
Qw $(kW.m^{-2})$	191.1	153.9	119.6	103.4	93.7

Discrepancies are provided in table 3. The duplication of the heat flux and the boundary layer thickness presents a maximum gap of 9%. The flight condition factor is well reproduced with a difference of 3% for case 1 and less than 1% for the others. As it represents the time scale of the flow, the Damköhler number is naturally very well duplicated. However the total enthalpy at the wall is not reproduced as well as other parameters. For instance, differences can reach more than 10% for case 1, but it can be as low as 6% in case 5. Hence, the equivalent flat plates overestimate the total enthalpy at the wall.

For cases 1 and 2, both the boundary layer thickness and the heat flux are very well reproduced. However, for cases 3, 4 and 5, the heat flux becomes overestimated over the flat plate by 8.2% and the boundary layer thickness 8.4% lower than in IXV. Therefore, the evolution of the heat flux seems related to the boundary layer thickness.

DOI: 10.13009/EUCASS2017-495

Table 3: Comparison between the IXV flight and the equivalent flat plate simulations.

Case	**1**	**2**	**3**	**4**	**5**
s_{eq} (cm)	10.8	24.4	41.7	62.3	82.6
$\Delta f_c/f_c$ (%)	2.8	0.5	-0.1	0.5	1.0
$\Delta Da/Da$ (%)	-3.8	-0.4	1.4	-0.5	-1.7
$\Delta\delta_{b.l.}/\delta_{b.l.}$ (%)	0.4	2.5	6.6	8.4	8.7
$\Delta Ht_w/Ht_w$ (%)	-10.9	-8.9	-8.6	-7.9	-6.6
$\Delta Q_w/Q_w$ (%)	1.8	-1.0	-8.1	-8.2	-7.1
$\Delta\phi_{th}/\phi_{th}$ (%)	14	4	-7	-12	-6
$\Delta\phi_N/\phi_N$ (%)	-62	-42	-47	-49	-54
$\Delta\phi_O/\phi_O$ (%)	-7.7	-0.7	-4.9	1.1	-1.3
$\Delta\phi_{O_2}/\phi_{O_2}$ (%)	9.2	-0.6	-7.1	-0.8	-2.8
$\Delta\phi_{allspecies}/\phi_{allspecies}$ (%)	-26.3	-12.7	-14.1	-1.1	-5.5

The temperature profiles shown in figure 6 show good agreement between IXV and flat plate, especially at s = 40 cm. For cases 4 and 5, the equivalent flat plate temperature profiles slightly overestimate those of IXV. Interestingly, the non-dimensional temperature profiles converge to the distribution seen in figure 7. This lack of sensitivity may be due to the low Eckert number. Hence, the thermochemical phenomena prevail over the kinetic effects.

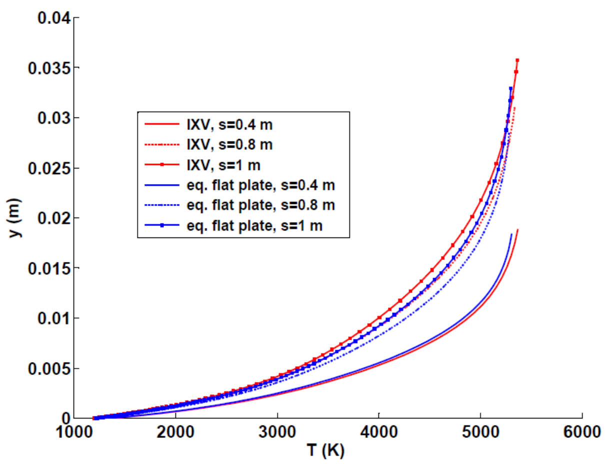

Figure 6: Temperature profiles for each point cases

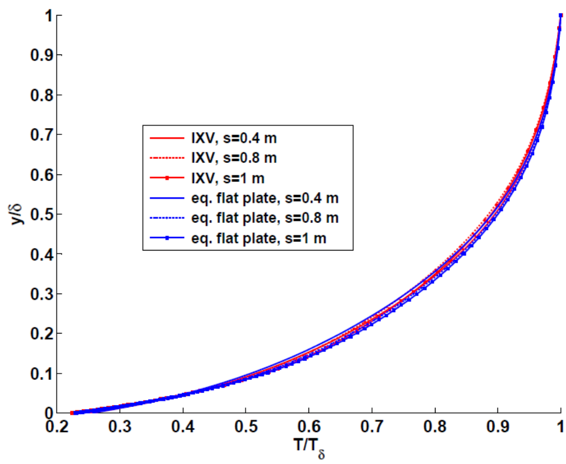

Figure 7: Non-dimensional temperature profiles for each point cases

However, such conclusion might not be enough because of the presence of pressure gradient. Indeed, the source term in the total enthalpy equation that depends on the pressure gradient might be non-negligible if the pressure gradient is too strong. To validate such hypothesis, the total enthalpy equation has been considered, and its non-dimensional form is written as:

$$\bar{\rho}\left(\bar{u}\frac{\partial \bar{H}_t}{\partial \bar{x}} + \hat{v}\frac{\partial \bar{H}_t}{\partial \hat{y}}\right) = E_c\left(\bar{u}\frac{\partial \bar{P}}{\partial \bar{x}} + \bar{\mu}\left(\frac{\partial \bar{u}}{\partial \hat{y}}\right)^2\right) + \frac{\partial}{\partial \hat{y}}\left(\frac{\bar{\lambda}}{Pr}\frac{\partial \bar{T}}{\partial \hat{y}} + \sum_{I=1}^{N}\frac{\bar{\rho}\bar{D}_I\bar{h}_I}{Sc_I}\frac{\partial Y_I}{\partial \hat{y}}\right) \tag{9}$$

The non-dimensional parameters are brought together in the table 4:

Table 4: Non dimensional parameters for the equation (9).

$\bar{x}$	$\hat{y}$	$\bar{u}$	$\hat{v}$	$\bar{\rho}$	$\bar{\mu}$	$\bar{\lambda}$	$\bar{D}_I$	$\bar{P}$	$\bar{T}$	$\bar{H}_t$
x/L	$\sqrt{Re}\,y/L$	u/u_δ	$\sqrt{Re}\,v/u_\delta$	ρ/ρ_δ	μ/μ_δ	λ/λ_δ	$D_I/D_{I,\delta}$	$P/\left(\rho_\delta u_\delta^2\right)$	$C_{p,\delta}T/h_\delta$	H_t/h_δ

Table 5 summarizes E_c and $E_c\partial\bar{P}/\partial\bar{x}$ and it shows that, in the present study case, the pressure gradient has a negligible impact on the boundary layer. Therefore the curvature of the IXV windward side, which induces a strong pressure gradient, has very few effects on the total enthalpy variation, concluding that the nature of the total enthalpy

DOI: 10.13009/EUCASS2017-495

boundary layer is mainly diffusive.

Table 5: Eckert number for each studied case.

Case	**1**	**2**	**3**	**4**	**5**
Eckert number E_c	0.025	0.082	0.111	0.111	0.114
$E_c \frac{\partial \bar{P}}{\partial \bar{x}}$	-2.2 × 10^{-2}	-4.9× 10^{-2}	5.0× 10^{-3}	3.0× 10^{-3}	3.0× 10^{-4}

The atomic and molecular nitrogen mass fraction profiles present discrepancies between the IXV and the equivalent flat plate which, in addition, increases close to the wall, as shown in figures 8 and 9, respectively. Particularly, the mass fraction of atomic nitrogen at the wall is lower on the IXV than over the equivalent flat plate. This could explain the overestimation of the contribution of the Nitrogen diffusion to the heat flux on the equivalent flat plate.

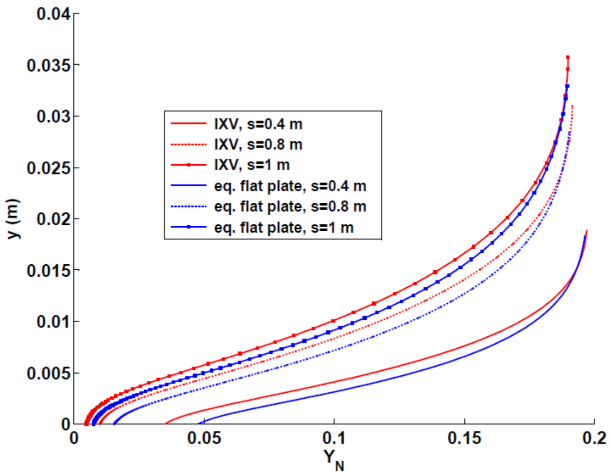

Figure 8: Mass fraction of N profiles.

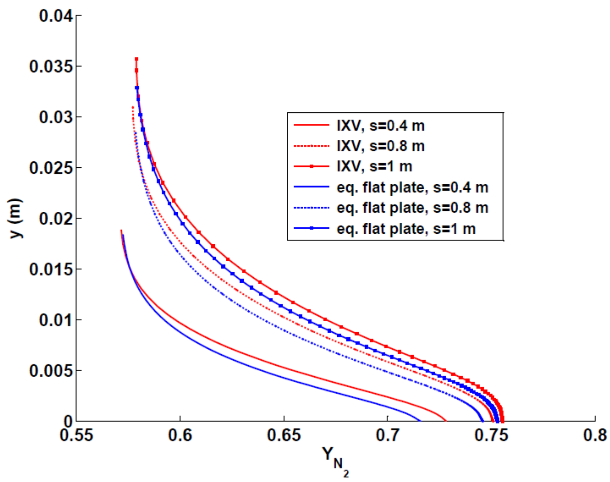

Figure 9: Mass fraction of N_2 profiles.

For the oxygen species: O, NO, O_2 (figures 10 and 11), the mass fraction matching between the equivalent flat plate and the IXV seems good whereas the N and N_2 are species which are very sensitive to thermochemical phenomena involved in the flow.

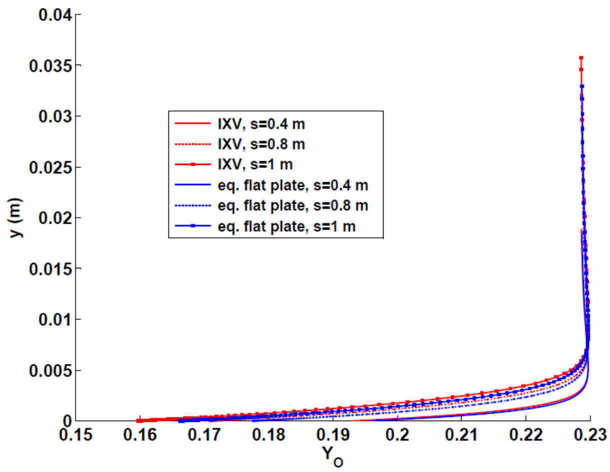

Figure 10: Mass fraction of O profiles.

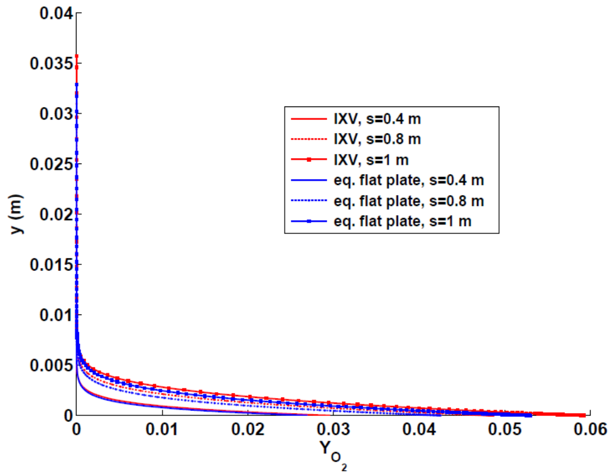

Figure 11: Mass fraction of O_2 profiles.

DOI: 10.13009/EUCASS2017-495

6.2 Off-stagnation methodology

The scaling step of the off-stagnation extrapolation methodology is applied for cases where the first step is most successful. Barbante[3] has shown that the outer edge velocity duplication requirement could be relaxed to reduce the length of the flat plate as the Eckert number is very low (table 5). This means that the thermochemical effects prevail over the kinetics ones in the boundary layer.

The flat plate available for the Plasmatron wind tunnel is 24 cm long and 2.5 cm thick (figure 12). The leading edge has a radius equal to 1.25 cm. The duplication is made at the trailing edge of the plate. Since the Plasmatron test model needs to be water-cooled, its thickness does not match the used for the equivalent flat plate in the previous simulations. This leads the end of the flat plate to be at a wall coordinate of 24.3 cm. Then, flow velocity in the Plasmatron is obtained by reproducing the parameter u_δ/x. The length x must be computed from the s_{eq} with the same method followed previously due to the significant difference of nose radius between the equivalent flat plate and the Plasmatron flat plate. Hence its expression is written as:

$$U_{pls} = L_{pls}\frac{U_\delta}{L_{eq}} \tag{10}$$

Where U_{pls} is the velocity in the Plasmatron facility and L_{pls} the length of the Plasmatron flat plate. U_δ is the velocity at the outer-edge of the boundary layer in the IXV and L_{eq} is the equivalent flat plate length for a specified s_{eq}. The boundary conditions are almost the same as those in the equivalent flat plates, except for the velocity value which is equal to the Plasmatron velocity reported in table 6. Here, the catalycity value is constant along the flat plate and the same as that was prescribed for the IXV.

The results of the heat flux duplication are given in table 7. The equivalent flat plate heat flux, compared with the Plasmatron flat plate, is overestimated by 6.6% for the case 3, and about 5.7% for 80 cm and 5.0% for the case 5. However, the duplication is reasonable as these heat flux differences are below 7%. The total enthalpy shows also a gap about 4.5%, which is lower than the obtained in step 1 due to the relaxation process of the velocity.

However, for cases 1 and 2, the velocity is very close to that of the equivalent flat plate. In fact, the length of the equivalent flat plate designed for the case 2 is equal to 24.4 cm, which is nearly the same as the length of the experimental flat plate (24.3 cm). For the case 1, as the measurement is done at s=12 cm instead of 24 cm, the Plasmatron velocity is very close to the equivalent flat plate case. Hence, the simulation results match perfectly.

Table 6: Plasmatron velocities for cases 1, 2, 3, 4 and 5.

Case	**1**	**2**	**3**	**4**	**5**
$U_{plasmatron}$ (m.s^{-1})	759.3[1]	1179.6	777.6	533.4	413.3

[1]The distance from the stagnation point is 12 cm instead of 24 cm because, as the equivalent length related to the case 1 is equal to 10.80 cm, the velocity should be equal to 1520 m.s^{-1}, which means a Mach number of M = 0.85. The flow is in transonic regime and the design does not fit with such conditions.

Table 7: Results of duplication from equivalent flat plate to Plasmatron test flat plate.

Case	**1**	**2**	**3**	**4**	**5**
$\Delta f_c/f_c$ (%)	-1.7	-0.4	1.2	-0.1	-1.1
$\Delta Da/Da$ (%)	3.4	0.8	-3.3	0.4	2.9
$\Delta Ht/Ht$ (%)	-0.4	0	3.5	4.4	4.9
$\Delta\delta_{b.l.}/\delta_{b.l.}$ (%)	-2.6	-2.6	-5.7	-4	-2.4
$\Delta Ht_w/Ht_w$ (%)	0.9	2.1	3.4	2.3	1.4
$\Delta Q_w/Q_w$ (%)	0.2	1.1	6.6	5.7	5.0

As the flight factor is reproduced, the Damköhler number is duplicated as well with a maximum gap around 3%. The profiles of species fraction, which are not shown here, are also well duplicated and in agreement with the theory.

7. Plasmatron experiments: expectations and results

The flat plate currently used in the Plasmatron is made of copper to improve the efficiency of the cooling system. However, to test TPS materials, an area of 18 cm long by 3 cm wide is left to insert a sample (figure 12), with the beginning of the sample set at 6.3 cm downstream of the stagnation point. This means that a catalytic jump will be enforced during the test in a shear flow configuration. For sake of realism, the mesh of the previous Plasmatron flat plate model is modified by splitting the wall in two parts with different catalycities. The first one is copper (γ = 0.1) and the other is the material sample, which has the same catalycity used for IXV simulations.

DOI: 10.13009/EUCASS2017-495

The off-stagnation methodology is applied to the equivalent flat plate with the catalytic jump. The new comparison of duplication parameters is shown on the table 8. The point chosen for the heat flux measurement over the experimental flat plate for the case 1 is put at 17 cm instead of 12 cm from the stagnation point to avoid excessive velocity discrepancies from the free-stream value. Hence the new value of velocity for the case 1 in the Plasmatron is $U_{pls} = 995.6$ m.s^{-1}.

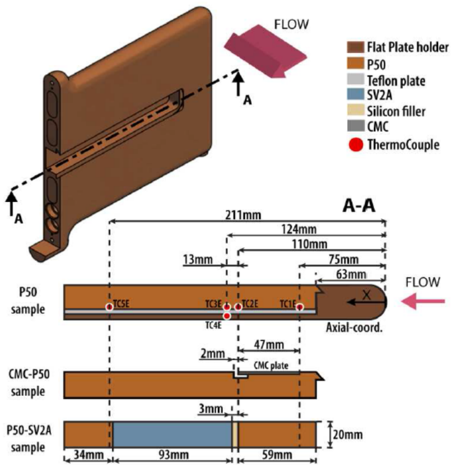

Figure 12: Experimental Plasmatron flat plate.[10]

Table 8: Results of duplication from equivalent flat plate to real Plasmatron test flat plate.

Case	1	2	3	4	5
$\Delta f_c/f_c$ (%)	-2.4	-2.0	0.2	-1.3	-2.3
$\Delta Da/Da$ (%)	3.4	3.9	-1.3	2.6	5.0
$\Delta Ht/Ht$ (%)	-1.5	0.1	3.6	4.6	5.3
$\Delta\delta_{b.l.}/\delta_{b.l.}$ (%)	-13.3	-10.5	-12.6	-7.8	-1.8
$\Delta Ht_w/Ht_w$ (%)	32.9	22.1	25.3	21.3	17.9
$\Delta Q_w/Q_w$ (%)	7.0	5.6	12.7	12.6	12.0

The equivalent flat plate heat flux is 12.7% higher than for the Plasmatron flat plate with the catalytic jump. This represents an increase of 6 points of the discrepancies considering the previous comparison case. The Damköhler number is reasonably duplicated for all cases with a maximum gap of 5%. The total enthalpy at the wall follows the same trend than the heat flux: the discrepancies increase sharply (32% for the case 1) and, therefore, such parameter is no longer properly duplicated. Such behavior contrasts with the ideal case proposed previously. Therefore, it would seem that the methodology is sensitive to catalytic transitions. Hence, the catalycity change affects significantly the energy distribution over the Plasmatron flat plate. The temperature profile and species profiles are no longer reproduced with a catalytic jump (figures 13 and 14).

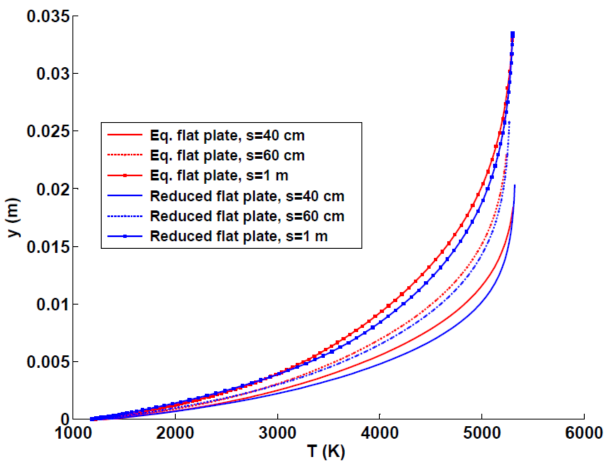

Figure 13: Temperature profiles for experimental flat plate case.

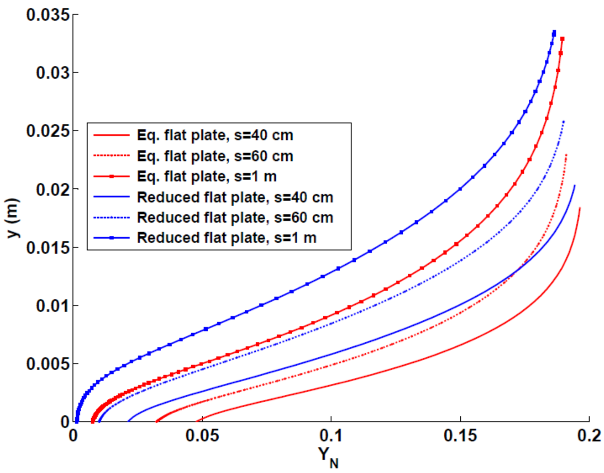

Figure 14: Atomic nitrogen mass fraction profiles for experimental flat plate case.

Over the Plasmatron flat plate, temperature is higher than over the equivalent flat plate, contrary to what is observed in the ideal Plasmatron flat plate case. Even though the Damköhler number seems correctly reproduced at the outer edge of the boundary layer, the species profiles show significant discrepancies. The oxygen species do not have the profiles reproduced, as seen in figure 15. The oxygen mass fraction is higher on the equivalent flat plate than over the experimental flat plate, and the same is observed for nitrogen. Hence, since temperature and species profiles are not reproduced, the wall total enthalpy is not duplicated.

DOI: 10.13009/EUCASS2017-495

Downstream the catalytic jump, the heat flux is lower on the Plasmatron flat plate than the found on the equivalent flat plate, whereas the comparison shows the opposite upstream (figure 16). As compared with the equivalent flat plate, the mass fraction of dissociated species at the wall is lower on the real flat plate, the catalytic recombination is less intense as well, increasing the heat flux duplication discrepancies (table 8).

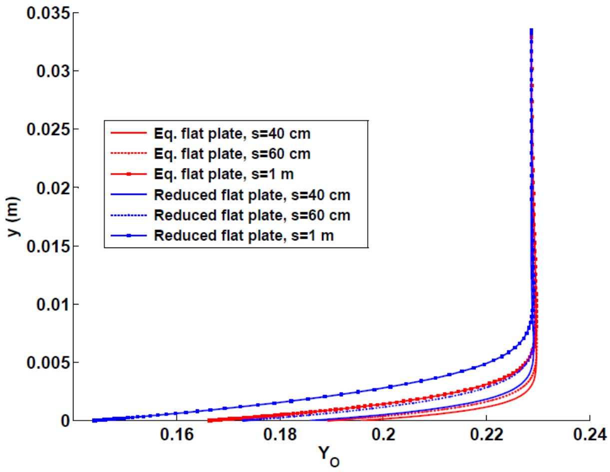

Figure 15: Oxygen mass fraction profiles for experimental flat plate case.

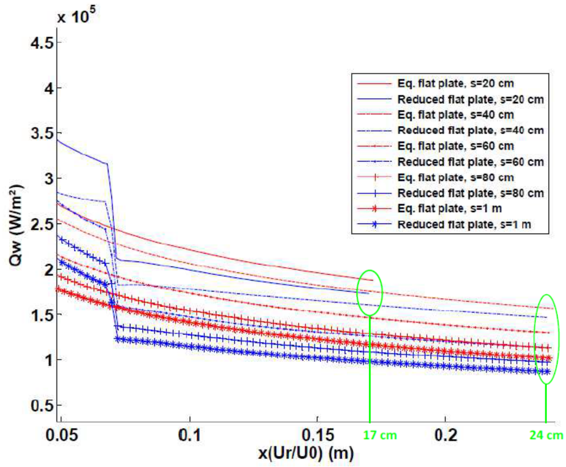

Figure 16: Heat flux comparison for experimental flat plate case.

In conclusion, the effect of the catalytic transition is significant over the experimental flat plate. The methodology could be improved by lengthening the experimental flat plate and having measurement points farther downstream the catalytic jump.

8. Global comparison of the heat flux between the IXV flight and the Plasmatron facility

The heat flux extrapolation from flight to an equivalent flat plate has presented few discrepancies (< 10%). Hence, considering the previous studies, the direct heat flux duplication can be attempted from IXV flight to Plasmatron facility. Not only sample points on the IXV vehicle have to be chosen, but also the measuring locations over the experimental flat plate. Then, the Plasmatron velocity condition has to be determined with:

$$u_{in,pls} = x_{pls} U_{IXV}^2 \frac{\rho_{IXV}\mu_{IXV}}{\xi_{IXV}} \tag{11}$$

Choosing the same sample points and the same IXV measurement points as before (with x_{pls} = 17 cm for the case 1), the velocities in the Plasmatron for each case are provided in table 9, and the extrapolation results are shown in the table 10.

Table 9: Plasmatron velocities for cases 1, 2, 3, 4 and 5.

Case	1	2	3	4	5
$U_{plasmatron}$ (m.s^{-1})	995.5	1179.6	777.6	533.4	413.3

Table 10: Comparison between the IXV flight data and the experimental flat plate results from direct duplication process.

Case	1	2	3	4	5
$\Delta f_c/f_c$ (%)	1.6	-1.5	-1.0	-0.6	-0.3
$\Delta Da/Da$ (%)	-2.6	3.5	2.3	1.8	1.6
$\Delta\delta_{b.l.}/\delta_{b.l.}$ (%)	-14.2	-7.8	-4.0	1.0	6.3
$\Delta Ht_w/Ht_w$ (%)	17.2	10.8	12.6	11.2	10.3
$\Delta Q_w/Q_w$ (%)	9.4	4.6	5.0	5.6	6.5

The outer-edge parameters, temperature, pressure, N, O and N_2 mass fractions are very well duplicated with a maximal discrepancy equal to 2.20%. The flight condition factor and the Damköhler number are also well reproduced with a maximum difference of 1.63% for the former and 3.5% for the latter. Results lead to significant differences in total enthalpy at the wall (17.2%) and below 10% in heat flux.

DOI: 10.13009/EUCASS2017-495

9. Conclusion

The paper aims at defining an experimental strategy for duplicating the heat flux from a configuration in flight to a ground test in the Plasmatron facility, on a complex configuration such the IXV. The methodology is applied in two steps:

- Data extrapolation from flight to equivalent flat plates
- Application of the off-stagnation methodology upon the equivalent flat plates

Five points over the surface of the IXV have been taken for the study at s = 20 cm, 40 cm, 60 cm, 80 cm and 1 m. The heat flux is very well extrapolated for cases 1 and 2. For the other cases, the equivalent flat plates overestimate the heat flux with a maximum gap of 8.2% which is considered as a reasonable extrapolation. The curvature of the IXV windward side does not affect the heat flux through the pressure gradient. Hence the total enthalpy boundary layer is mainly diffusive.

Considering the actual design of the experimental flat plate, the duplication methodology is applied to assess the differences from the theoretical duplication methodology. Contrary to the theoretical case, the wall total enthalpy is not well reproduced. The underestimation of the heat flux observed with the theoretical application of the off-stagnation methodology increases until 12%. The direct duplication is also applied to assess the global error from flight to Plasmatron facility using the real experimental flat plate. The global differences do not exceed 10% for the case 1 and 7% for the other cases.

Therefore, the presented extrapolation methodology can duplicate the heat flux, from a re-entry body flight to Plasmatron testing facility, with a reasonable accuracy allowing a better design for TPS. Nevertheless, its actual efficiency must be assessed by an experimental validation of the methodology which will be implemented in future investigations. Furthermore, the methodology has to be applied for other flight cases and shapes to define the range of its application.

However, some discrepancies may come from the physical and numerical models used in the extrapolation methodology:

- The thermal and mass diffusion phenomena govern the heat flux but, the transport of species in the high velocity part of the boundary layer may alter the mass fraction diffused to the wall, because of the consumption history of species, providing less fuel to the catalytic wall.
- The diffusion model used in this project is the Fick's law which considers only binary diffusion. The model could be improved to have a more realistic distribution of species in the reacting boundary layer. Besides, the shock layer is assumed only in chemical non-equilibrium. Chemical reactions happen but the flow remains in thermal equilibrium. For other flight case, thermal non-equilibrium flow could appear if the Knudsen number were higher than 10 and its effects on the extrapolation process must be therefore assessed.

References

[1] Sarma G. S. R. Physico-chemical modelling in hypersonic flow simulationl. *Progress in Aerospace Sciences*, 36(3–4):281–349, 2000.

[2] Kolesnikov A. F. Extrapolation from high enthalpy tests to flight based on the concept of local heat transfer simulation. Technical report, Institute for Problems in Mechanics RAS, Prospect Vernadskogo 101/1, 117526, Moscow, Russia, October 1999.

[3] Barbante P. F. Heat flux duplication between ground facility and hypersonic flight. *Journal of Thermophysics and Heat Transfer*, 23(4), October–December 2009.

[4] Viladegut A. and Chazot O. Off-stagnation point testing in plasma facility. volume 7, pages 113–122. EUCASS Proceedings Series – Advances in AeroSpace Sciences, 2015.

[5] Fay J. A. and Riddell F. R. Theory of stagnation point heat transfer in dissociated air. *Journal of the Aeronautical Sciences*, 25(2):73, February 1958.

DOI: 10.13009/EUCASS2017-495

[6] Goulard R. On catalytic recombination rates in hypersonic stagnation heat transfer. *Journal of Jet Propulsion*, 28(11):737–745, 1958.

[7] Chazot O. Panerai F. and van der Haegen V. Aerothermochemistry testing for lifting reentry vehicles. *7th European Symposium on Aerothermodynamics Proceedings*, (Id. 48.5.2011).

[8] Ledard N. Preliminary study of a new method of extrapolation to flight for plamsatron wind tunnel. Short-training report, 2015-45, von Kármán Institute for fluid dynamics.

[9] Park C. Review of chemical-kinetic problems of future nasa missions, i: Earth entries. *Journal of Thermophysics and Heat Transfer*, 7(3), July-Sept 1993.

[10] Ceglia G. Trifoni E. Gouriet J.B. Chazot O. Mareschi V. Rufolo G. and Tumino G. Off-stagnation tests of esa ixv tps interfaces in plasmatron. *8th European Symposium on Aerothermodynamics for Space Vehicles*, March 2–6 2015.